

[UC]

An altimetric and bathymetric study of elastic thickness in the central Pacific Ocean

Andrew M. Goodwillie and A.B. Watts

Department of Earth Sciences, University of Oxford, Parks Road, Oxford OX1 3PR, UK

Received March 24, 1993; revision accepted May 21, 1993

ABSTRACT

Using a 1-D spectral approach we recover the underlying topography across ten seamounts in the south central Pacific Ocean from high-resolution along-track satellite altimetry data, this in turn yields an estimate for the elastic thickness value. Theoretical modelling showed that after correcting for the effects of one-dimensionality, this approach can clearly indicate areas of low elastic thickness values. Our results show that whilst a number of the seamounts in this region display anomalously low elastic thickness values, some of the seamounts studied have values close to those expected. Coupled with the results from geochemical and heat flow studies, this suggests that the region of low elastic thickness values is not as extensive as previously thought.

1. Introduction

Oceanic flexure studies [1] show that the elastic thickness of the lithosphere increases with age, corresponding approximately to the depth to the 450°C isotherm. Elastic thickness estimates beneath seamounts in the south central Pacific Ocean, however, indicate that the flexural rigidity in this region is weaker than expected [2,3]. Although no unusually high heat flow measurements have been found for this area [4], these low flexural rigidities have been explained by McNutt and Judge [5] in terms of enhanced heat flux into, and low viscosity below, a thin (~75 km) cold thermal boundary layer and they suggested that small-scale convective instabilities maintain the shallow plate thickness. This model provides a link with a number of other anomalous observations for this region: the depth to the sea floor is unusually shallow [6]; there is a high concentration of hotspots [5]; the rate of subsidence due to cooling of the oceanic lithosphere is lower than expected [7]; the occurrence of lineated gravity anomalies oriented roughly parallel to the direction of absolute plate motion [8]; and Love-wave phase velocities are low across this region [5,9]. These observations point to an anomalously hot upper mantle compared to normal oceanic areas.

Additionally, rocks from a number of islands have been found to display unexpected isotope and trace element ratios [10,11].

The flexural studies of Calmant [2] and Calmant and Cazenave [3], which indicated the low flexural rigidity in this region, concentrated upon 18 seamounts in the Society Islands, the Cook–Austral chain, the Marquesas Islands and the Tuamotu archipelago. The data used by these authors were the National Oceanographic and Atmospheric Administration's gridded Synthetic Bathymetric Profiling System (SYNBAPS) and Seasat altimetry data. They forward-modelled the 2-D geoid surface over this gridded bathymetry and compared the result with a 2-D geoid surface constructed from Seasat data. By adjusting parameters in the model to minimise differences between the two geoid surfaces, they were able to estimate the elastic thickness of the oceanic lithosphere. However, as pointed by these and other workers [e.g., 12], the SYNBAPS data contain some serious errors, with amplitude errors commonly exceeding 1 km and location errors of up to several nautical miles. Graphic examples of obvious discrepancies in the SYNBAPS data are given by Smith and Wessel [13]. Errors in the gridded bathymetry, which forms the basis of the forward modelling, will lead to errors in the final results.

Forward modelling of the geoid over features in areas of poor bathymetric coverage is therefore difficult. Further, the Seasat data are relatively noisy and irregularly-spaced which leads to a variable-quality geoid surface.

This forward-modelling method is in common with much of the earlier work that incorporated altimetry data into flexural studies—the available bathymetric data was forward-modelled to produce the geoid which was then compared to that derived from the altimeter data [e.g., 14–16]. A number of studies however, have attempted the inverse problem, that of using the altimeter data to directly predict sea floor bathymetry [e.g., 17–22].

The objective of this paper is to re-examine the low elastic thickness values in the south central Pacific Ocean by using a method in which the along-track bathymetry is predicted directly from the altimetry data. In particular, our method differs from the forward-modelling method described above in two ways:

(1) Processed along-track satellite altimeter data have a resolution of approximately 14 km, i.e., twice the spacing between data points, whereas the across-track resolution is generally much poorer. For a typical region in our study area, a combined plot of ERS-1, Geosat and Seasat satellite ground tracks shows that the separation between adjacent tracks may be as large as 75 km giving an across-track resolution of just 150 km. Clearly, if a 2-D geoid anomaly surface is calculated from such a data distribution, the resolution will vary greatly according to position. We therefore chose not to construct a 2-D geoid surface and instead we use the uniformly high-resolution data along individual satellite arcs.

(2) Ship track coverage in the south central Pacific Ocean is generally sparse and forward modelling over such a bathymetry will lead to a smoothed, low-resolution geoid. In contrast, our method uses the observed bathymetry to *constrain* the recovery of predicted along-track bathymetry.

2. Lithospheric flexure

Short-wavelength gravity and geoid anomalies are highly correlated with sea floor topography [23] whereas long-wavelength anomalies (≥ 1000

km) are produced by deeper processes in the earth such as mantle convection [24,25]. By subtracting a spherical harmonic reference field to a particular degree and order to remove the well-determined longer wavelength features, the marine geoid can be used to gain information on the mechanical properties of the oceanic lithosphere, namely flexural rigidity. The relationship between a load on the sea floor and the resultant geoid anomaly depends upon the compensation of the load.

Watts [1] used a linear expression, $g(x) = f(x) \cdot b(x)$, relating gravity and bathymetry, where $g(x)$ is the observed gravity anomaly profile, $b(x)$ is the observed bathymetric profile, and $f(x)$ is the filter function that converts the observed bathymetry into a profile resembling the observed gravity anomaly. The filter, $f(x)$, therefore contains information on the state of compensation of the bathymetry. By working in the wavenumber domain, this convolution becomes a multiplication:

$$G(k) = Z(k) \cdot B(k) \quad (1)$$

where $G(k)$, $B(k)$, and $Z(k)$ are the Fourier transforms of the gravity, bathymetry and filter function respectively and k is the wavenumber, defined as $k = 2\pi/\lambda$. The Fourier transform of the filter function, $Z(k)$, is called the gravitational admittance and has the form of a bandpass filter. For a flexural plate model having a two-layer crustal structure in which layer 2 overlies a denser layer 3, Watts and Daly [26] gave the gravitational admittance as:

$$Z(k) = 2\pi G(\rho_{\text{load}} - \rho_w) e^{-kd} \times \left\{ 1 - \Phi(k, D) \left[\frac{(\rho_3 - \rho_2) e^{-k(t-t_3)} + (\rho_m - \rho_3) e^{-kt}}{(\rho_m - \rho_{\text{infill}})} \right] \right\} \quad (2)$$

where ρ_{load} , ρ_w , ρ_2 , ρ_3 , ρ_m , and ρ_{infill} are the densities of the sea floor topography, water, layer 2, layer 3, mantle, and of the material infilling the flexural moats, respectively; d , t and t_3 are the mean water depth, depth below the sea floor at which compensation occurs, and the thickness of layer 3, respectively, and G is the gravitational constant. The flexural response function, $\Phi(k, D)$, is defined as:

$$\Phi(k, D) = \left[\frac{Dk^4}{(\rho_m - \rho_{\text{infill}})g} + 1 \right]^{-1}$$

where g is the average acceleration due to gravity, and D is the flexural rigidity of the elastic plate given by $D = ET_e^3/[12(1 - \sigma^2)]$, in which E is Young's modulus and σ is Poisson's ratio. The strength of the elastic plate can be described in terms of the flexural rigidity, D , or, equivalently, by the thickness of the elastic plate, T_e , and either of these values can be used to infer the state of compensation due to loading.

Chapman [27] derived a simple relationship to convert between gravity and geoid values and this shows that the geoid admittance function, $Z'(k)$, may be given as $Z'(k) = Z(k)/g|k|$. Working directly with the geoid has the advantage of eliminating the extra processing steps that are required to calculate gravity from altimetry data. Clearly the function $Z'(k)$ blows up for small k and this singularity is avoided by, firstly, shaping $Z'(k)$ such that the smallest value of the wavenumber is $k = dk$ where $dk = 2\pi/N_d dx$ in which N_d is the number of discretely sampled data points spaced dx apart, and, secondly, by subtracting from the geoid signal those longer wavelengths defined by some reference model. The minimum value $k = dk$ corresponds to the total length of the space domain profile and is the maximum wavelength that need be considered. The maximum value of k is determined by the Nyquist frequency of the data and for short wavelengths the $Z'(k)$ filter is stable. Rearrangement of eq. (1) shows that topography may be recovered from the geoid if the admittance function is known:

$$B(k) = N(k)/Z'(k) \quad (3)$$

where $N(k)$ is the Fourier transform of the geoid. In this case it is at short wavelengths that the filter is unstable so any short-wavelength information in the input geoid signal is blown up when the signal is convolved with this filter. In order to avoid this instability it is necessary to either shape the filter to tail off at short wavelengths or, equivalently, to pre-filter the input geoid signal to remove these short wavelengths and it is this latter approach that we chose to adopt.

If, however, some information is already known about the bathymetry, $b(x)$, then eq. (3) can be used to find the most suitable admittance function that best matches the recovered bathymetry to that observed, i.e., an estimate for the elastic

thickness value can be obtained. This has important implications for bathymetric prediction particularly in areas where only a limited amount of bathymetric information is available and in this present study we use this method of bathymetric prediction to estimate the elastic thickness values beneath seamount loads.

3. Dimensionality

When using one-dimensional methods to model two-dimensional features there are necessarily limitations and we investigated their effects. From eq. (3) we forward-modelled the 2-D geoid anomaly over a gaussian-shaped seamount centred at the origin of an (x,y) coordinate system, and then recovered the 1-D topography from geoid anomaly profiles sampled along a track line that passes over the centre of the seamount along the x -axis.

We investigated the effects of using a model seamount that is gradually stretched out in the across-track (y) direction perpendicular to the track line. We define the "dimensionality" of a seamount in the same way as Watts et al. [28], that is, a circular seamount is taken to have a dimensionality of 1:1, an oval-shaped seamount that is three times wider in the across-track direction has a dimensionality of 3:1, and so on up to a dimensionality of infinity:1 which corresponds to a seamount stretched to infinity, i.e., a ridge trending in the y direction. In all cases the seamount is of gaussian cross-section in the along-track x direction.

The 1-D method of recovering topography from the geoid assumes that there is no contribution to the wavevector in the across-track direction such that $|k_y| = 0$, i.e., all features extend to infinity perpendicular to the track line. By using a 2-D seamount with dimensionality of infinity:1 in the forward modelling, this assumption is automatically satisfied and the topography recovered from a 1-D profile is identical to the model topography, providing that the same elastic thickness values are used.

However, for seamounts having a dimensionality other than infinity:1 the condition $|k_y| = 0$ breaks down. For these cases, if the elastic thickness used to recover the topography is set to the same value as that used in the initial 2-D forward

modelling, then the amplitude of the recovered topography is always less than that of the model seamount. This is implicit in the 1-D calculation which assumes that the excess mass producing the geoid anomaly stretches to infinity perpendicular to the track line and thus a lesser amount of topography is required to create any given anomaly. Evidently, the greater the departure of dimensionality from infinity:1, the greater is the discrepancy in amplitude between the recovered and model topographies. The peak amplitude of the recovered topography can be matched to that of the model by using lower values of T_e in the 1-D topographic recovery calculation. The elastic thickness value that most closely matched the peak amplitudes of the two topographies was defined as T_e^{rec} and in all cases where dimensionality infinity:1, T_e^{rec} was lower than the true elastic thickness value, T_e^{true} , as shown in Fig. 1. From this figure it is seen that for low elastic thickness values the curves converge and, further, for seamounts with dimensionality $> 1:1$, T_e^{rec} curves lie close to the T_e^{true} line (i.e., within 5 km) for $T_e^{\text{true}} \leq 30$ km.

Few of the real satellite profiles used later in this study may actually pass over the centre of the seamounts and so in Fig. 1 we also present results (dashed lines) showing the effect of profiles passing over the flank of the model seamount. For this, profiles were sampled at a distance of 13.6 km (twice the along-track data point spacing) from the centre of the seamount, parallel to the x -axis. For a large seamount of halfwidth 60 km (Fig. 1a), the geoid profiles, recovered topographic profiles and T_e^{rec} curves are almost identical to those obtained over the centre of the seamount. Again, for seamounts having dimensionality $> 1:1$ the T_e^{rec} curves converge for $T_e^{\text{true}} \leq 30$ km. For a smaller model seamount having a halfwidth of 30 km, a value thought to be similar to that for many of the south central Pacific seamounts, the effect of dimensionality upon the T_e^{rec} curves is more pronounced as shown in Fig. 1b. For dimensionality $> 1:1$, these curves converge for $T_e^{\text{true}} 15$ km, about half the value for the larger model seamount.

The main excursions from the T_e^{true} curves are evident for models in which the T_e^{true} used in the 2-D forward modelling is high, and in which the dimensionality of the model seamount is 1:1 or

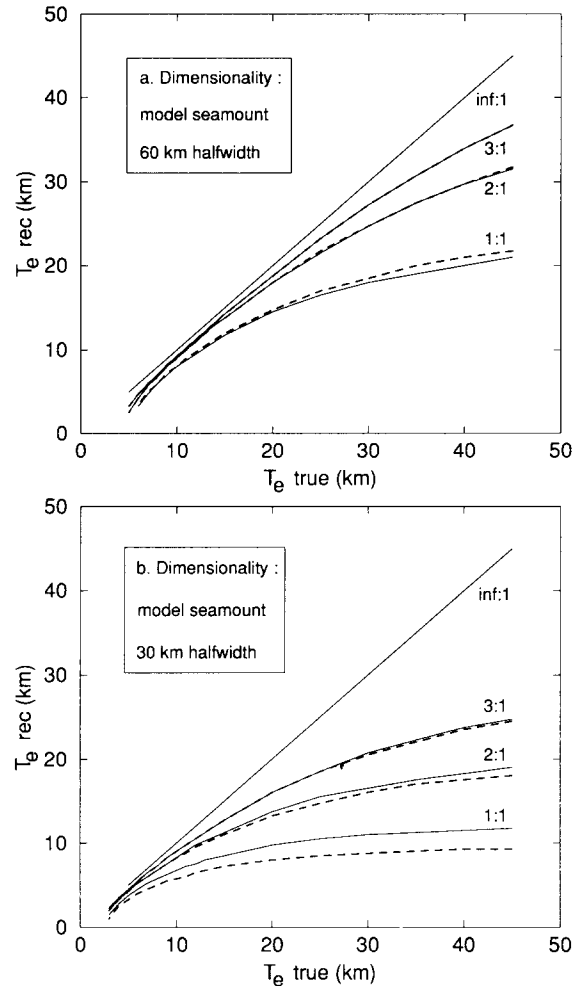


Fig. 1. Curves showing the elastic thickness values, T_e^{rec} , used in the 1-D topographic calculation that are required to match the amplitudes of the recovered 1-D topographic profiles with those of the 2-D model. The figures on the right of each curve give the dimensionality of the 2-D model seamount used to forward model the geoid anomaly. Solid lines show elastic thicknesses for profiles passing over the centre of the model seamount, dashed lines are for profiles passing over the flank of the model seamount at a distance of 13.6 km from the centre. The horizontal axis gives the elastic thickness value, T_e^{true} , used in the 2-D forward modelling and the vertical axis is the elastic thickness, T_e^{rec} , used in the 1-D topographic recovery calculation. Model seamounts had halfwidths of (a) 60 km, and (b) 30 km.

less. For the south central Pacific Ocean, previous studies have indicated that T_e values across the region are anomalously low, with T_e generally less than 15 km [2]. Bathymetric maps indicate

that most of the seamounts used in this paper have a dimensionality of approximately 1:1 which will limit the preciseness of our results.

Finally, the effect of 1-D modelling upon the shape of the recovered topography is given in Fig. 2 for a seamount of halfwidth 30 km. In all cases, these profiles show that the widths of the recovered topographies are all almost identical to the model widths. Low T_e^{rec} values produce side lobes since the 1-D calculation recovers the topography that would best create the given geoid anomaly.

Importantly, these profiles show that for both the along-axis and off-axis track lines, the character of the recovered topography is close to that of the model topography.

Modelling has shown that discrepancies do exist between the 1-D and 2-D cases but, as shown in Fig. 1, these discrepancies are small for seamounts in an area of low regional modelled T_e values. The modelling also showed that the character and shape of the 1-D recovered topographic profiles were very similar to those of the models.

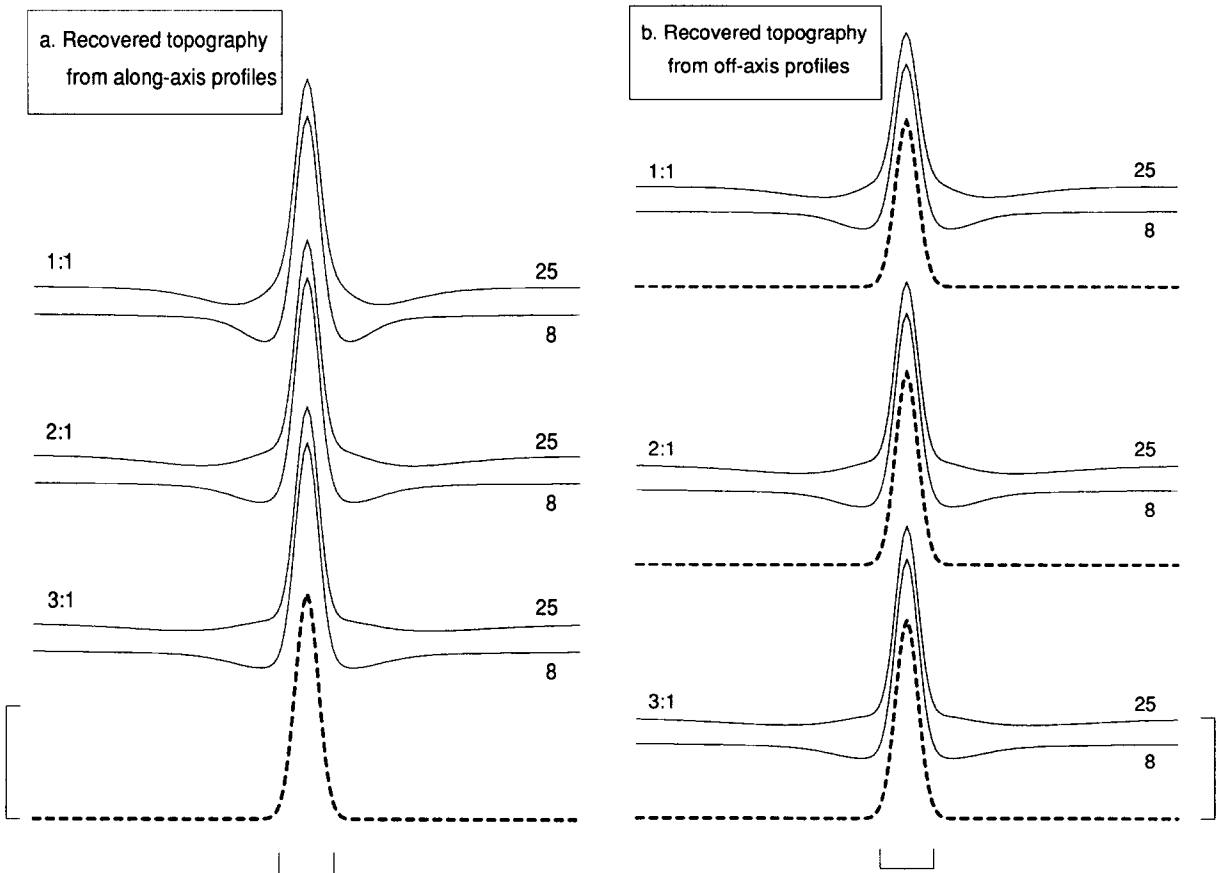


Fig. 2. 1-D topographic profiles (solid lines) recovered from geoid anomaly profiles sampled over a 2-D model seamount with gaussian cross-section of halfwidth 30 km and peak amplitude 4000 m. For different dimensionalities, labelled on the left hand side, the 2-D geoid anomaly over the model seamount was forward modelled for T_e^{true} values of 25 and 8 km, approximately corresponding to off-ridge and on-ridge volcanism, respectively [23]. For each case shown, the recovered 1-D topographic profiles were calculated using the T_e^{true} value that best matched the peak amplitudes of the recovered and model topographies. The horizontal scale bar represents a distance of 100 km and the vertical scale bar represents a topography of 2000 m. (a) Topography recovered from profiles passing over the centre of the seamount. The model topography lying beneath the track line was identical in each case, having a constant peak amplitude of 4000 m (single lower dashed line). (b) Topography recovered from profiles passing over the flank of the seamount 13.6 km from the centre. For these off-axis profiles, the model topography (dashed lines) varies with dimensionality such that the smallest peak amplitude is for a 1:1 model seamount and the largest, which is identical to the central peak amplitude (4000 m), is for the seamount having dimensionality of infinity: 1.

4. Data

4.1 Satellite data

The satellite altimetry data used in this paper comprised along-track ERS-1, Geosat and Seasat mean sea surface height measurements. After correction for atmospheric and oceanic effects these data closely correspond to the marine geoid. The Geosat data from the Exact Repeat Mission (ERM) [29] consist of data resampled at 1 s intervals and were averaged over sixty 17-day repeat cycles. These data contain very little noise (Fig. 3) and no subsequent filtering was required; topography recovered from these data was not contaminated by amplified high-frequency noise. The Seasat altimeter data comprise individual, irregularly-spaced cycles in which each data point has an accuracy of approximately 10 cm [30]. This much higher level of noise is clearly seen in both the along-track geoid profile and its power spectrum as shown in Fig. 3. Care must be taken to avoid this noise being blown up and for Seasat data it was necessary to pre-filter the mean sea surface height measurements. For this purpose a gaussian filter of halfwidth 22.5 km (approximately $3 \times$ sampling interval) was effective in suppressing this short-wavelength noise. Where possible, use was made of the higher-inclination ERS-1 satellite data from the ongoing Multi-disciplinary phase of its mission [31], which, with a 35-day repeat cycle, gives a ground track density twice that of the Geosat ERM data. Like the Geosat data, the ERS-1 data were resampled from the original 0.1 s points to 1 s intervals and were averaged over five 35-day repeat cycles supplied by the European Space Agency. The typical noise level associated with the data was found to be intermediate to that of the Geosat and Seasat data (Fig. 3) and the mean sea surface height measurements were pre-filtered with a gaussian filter of halfwidth 15 km (approximately $2 \times$ sampling interval).

4.2 Ship data

Surface ship bathymetric data are used to constrain the topographic modelling and therefore play a crucial role in this study. In place of the SYNAPS data, we constructed our own gridded

bathymetric data sets from the original ship leg data residing in the Oxford marine database. Of these, 81% of the cruises were carried out since 1967, the year when satellite navigational aids became available. Crossover error analysis of bathymetric data falling within a $10^\circ \times 10^\circ$ box centred upon each seamount pinpointed poor-quality data that needed to be removed and fathom-to-meter scaling differences, therefore allowing the overall data quality to be improved. These depth data were then combined with coastline data before being binned and gridded at 2.5 min intervals using a continuous curvature algorithm [13] to produce a bathymetric database for that seamount.

5. Recovery of along-track bathymetry

Seamounts selected for this study satisfied the following three criteria: the occurrence of satellite altimeter data within a few kilometers of the seamount; the availability in the database of surface ship bathymetric measurements lying close to the seamount; and the availability of age data for both the seamounts and the underlying sea floor.

After removal of the GEMT1 reference field [32] up to degree and order 36, the mean sea surface height measurements along individual satellite arcs were resampled at 6.8 km intervals in order to interpolate over any data gaps that may have been present. The data were then detrended and tapered at the ends to avoid edge effects. Only satellite arcs that contained no missing raw data points directly over the seamount were used since it is precisely these points that define the amplitude of the anomaly.

Sampling the gridded bathymetric databases at the same position as the altimeter data points yielded bathymetric profiles which we take to be the "observed" profiles. Smooth profiles reflected a low density of ship track coverage in the area whilst profiles showing shorter wavelength detail indicated more densely surveyed areas. The water depth, d , around each seamount was estimated from the observed bathymetry to the nearest 100 m. As the regional depth for much of the study area is of the order of 4000 m, the major part of the seamounts and volcanoes is submerged and is taken to consist of submarine

basalt. On the basis of gravity and borehole estimates, Hyndman et al. [33] concluded that the mean density of submarine basalt is about 2800

kgm^{-3} , and this was the value we used for the load density, ρ_{load} . In eq. (2), the buoyancy term given by $(\rho_m - \rho_{\text{infill}})g$ assumes that the flexural

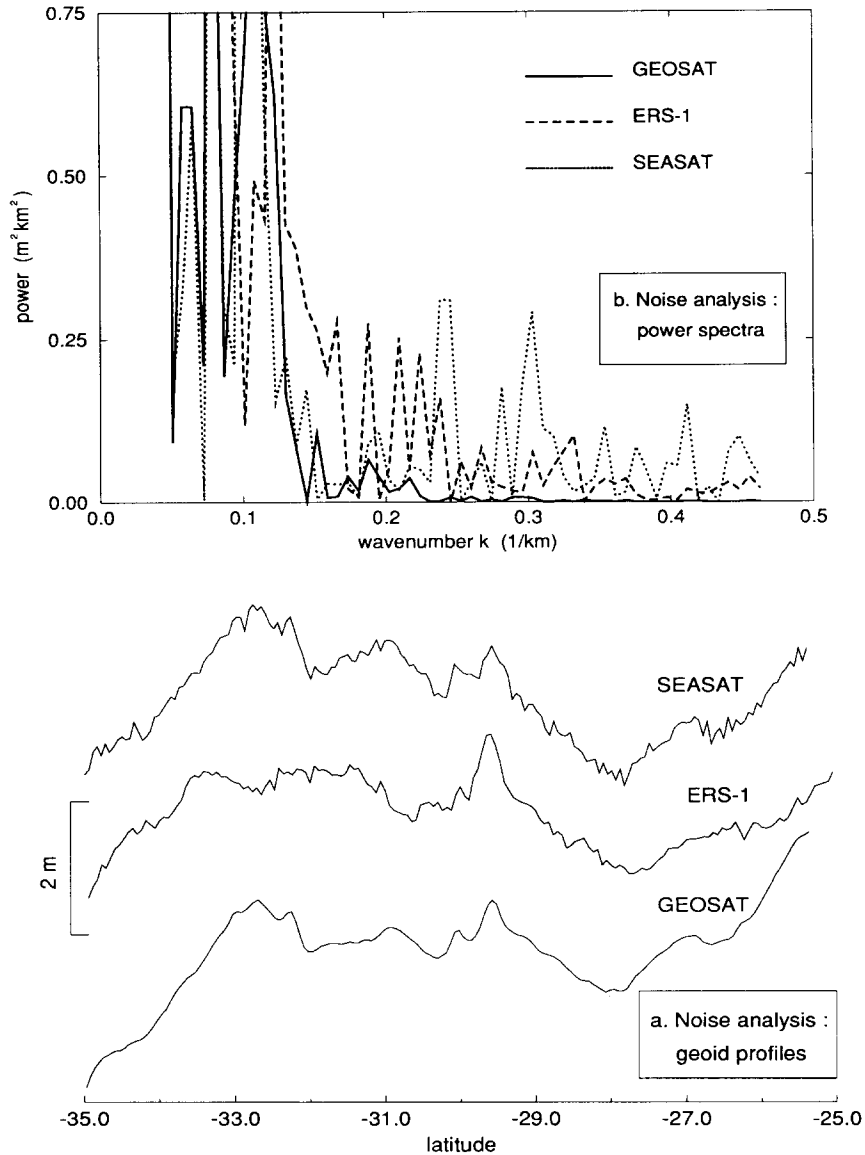


Fig. 3. The typical levels of noise associated with the unfiltered satellite altimetry data were obtained in an area of the south central Pacific devoid of large seamounts and other obvious tectonic features. The area chosen lay between the Austral and “A” fracture zones, bounded by the geographical box 195–205° longitude and 35–25°S latitude. Here, descending satellite tracks Geosat d042 and Seasat R0718 are coincident and the higher angle ERS-1 d358 intersects these and lies within 100 km at its ends, therefore allowing these three tracks to be compared. (a) Unfiltered along-track geoid anomaly profiles after removal of the GEMT1 reference field up to degree and order 36 [32]. The averaged Geosat data show little short wavelength noise and the profile appears smooth. The effect of noise causes the profiles to lose this smooth appearance and is visible on the ERS-1 profile but is most clear on the Seasat profile. (b) The power spectra of the unfiltered geoid profiles shows the noise levels associated with the three data sets more distinctly. At large wavenumber the power in the Seasat data (dotted line) is clearly and consistently higher than that in both the ERS-1 (dashed line) and Geosat (solid line) data. The high quality of the Geosat data is reflected in there being virtually no power in the signal at shorter wavelengths ($k > 0.15 \text{ km}^{-1}$).

TABLE 1

Values of the constants used to recover topography from geoid anomaly profiles

Constant	symbol	value	units
Young's modulus	E	70	GPa
Poisson's ratio	σ	0.25	
Average gravity	g	9.81	ms^{-2}
Gravity constant	G	6.673×10^{-11}	$m^3kg^{-1}s^{-2}$
Density of layer 2	ρ_2	2800	kgm^{-3}
Density of layer 3	ρ_3	2900	kgm^{-3}
Density of mantle	ρ_m	3330	kgm^{-3}
Thickness of layer 3	t_3	3500	m
Thickness of crust	t	5000	m
Density of load	ρ_{load}	2800	kgm^{-3}
Density of water	ρ_w	1030	kgm^{-3}

moat around the seamount is completely infilled with material of density ρ_{infill} . Flexural moats gradually become infilled with debris and detritus eroded off the seamount and with deep-sea sediments and since the moat is cored by the base of the load, the infill density will have a value lying between the density of the load, ρ_{load} , and that of the eroded material. Watts and Ten Brink [34] successfully modelled flexure under the Hawaiian Islands using infill densities of 2300–2600 kgm^{-3} which are consistent with velocities inferred from seismic refraction data. Since none of the seamounts used in the present study were associated with pronounced moats, we expect our best-fitting infill density to be in a similar range.

Using eq. (3) and the values of constants given in Table 1, the geoid anomaly profiles were used to recover topography underlying the satellite ground track. Each recovered topographic profile was compared with the detrended observed profile and the values of the ρ_{infill} and T_e parameters in the 1-D recovery computer program were adjusted until the best match between the observed and recovered topographies was obtained.

The best-fitting profile was determined visually such that the amplitude, flanks, and overall character of the recovered topography most closely matched that of the available topography. There were two reasons for determining the best-fit profiles visually.

(1) That due to the relatively sparse ship track coverage in this area of the south Pacific; for

example, a seamount close to the one under investigation may not have been surveyed bathymetrically and so produces no topography on the observed bathymetry profile. The satellite altimeter, however, may measure the geoid anomaly over this secondary feature and so recovers topography at this position. Any automatic procedure that calculates the *rms* difference between the two profiles would therefore be biased by this rogue secondary seamount and a good fit to the main seamount could very well be offset by a few bad points such as these elsewhere on the profile. The only way to avoid this would be to place little weight on the *rms* differences over such features, giving heavier weighting to the main seamount.

(2) Although the ground tracks of descending arcs, particularly ERS-1, may be subparallel to ridge sections of the East Pacific Rise, these tracks will transgress oceanic isochrons, and cross fracture zones and topographic loads of different ages. This means that the T_e value will necessarily vary along each individual profile and over each seamount studied. Since the amount and extent of the any weighting would, in these cases, be a subjective process, visual determinations around the seamount of interest were considered superior.

6. Testing the bathymetric recovery method

To test the one-dimensional modelling method we chose to study the 3800 m high Great Meteor Seamount in the central Atlantic Ocean for which two estimates of elastic thickness have previously been published [35,36] and for which good surface ship bathymetric data already exist. Recovered 1-D topographic profiles will therefore be well constrained by these high-density bathymetric data allowing a direct comparison between the 1-D method presented here and the 2-D gravity modelling method used by earlier workers.

Ascending ERS-1 track a017 passes over the centre of the seamount and records a pronounced geoid anomaly with amplitude 6.7 m. Best-fitting recovered topographic profiles were obtained for values of ρ_{infill} between 2400–2600 kgm^{-3} and values of T_e^{rec} between 9–13 km and for one such best-fit profile shown in Fig. 4, the amplitude, flanks and width of the Great Meteor Seamount are recovered extremely well. The

range of acceptable T_e^{rec} values obtained by 1-D modelling can be used in conjunction with Fig. 1a, which is for a model seamount of similar dimensions, to correct for the effects of 1-D mod-

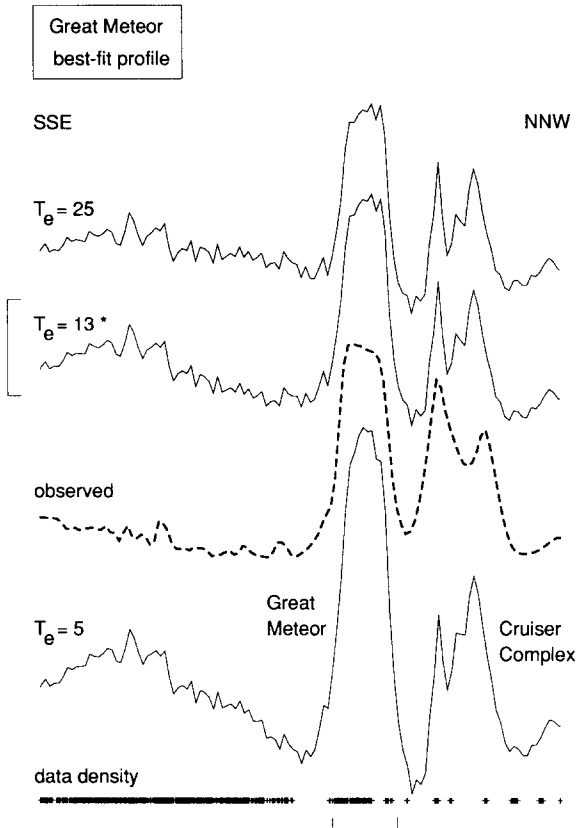


Fig. 4. Best-fit topographic profile for the Great Meteor Seamount recovered from ERS-1 track a017. The dashed profile shows the observed bathymetry sampled directly beneath the track line. The uppermost and lowermost of the solid profiles shows the recovered topography for elastic thicknesses of 25 and 5 km. The remaining solid profile, indicated with an asterisk, shows the best-fit topography recovered for $T_e^{\text{rec}} = 13$ km. The line of small crosses plotted below the stack of profiles gives the density of observed ship track bathymetric data lying within ± 7.5 km of the ERS-1 satellite ground track. The difference in elastic thickness between the Great Meteor Seamount and the Cruiser Complex was shown by Verhoef [36] to be of the order of 10 km and this, coupled with the sparse bathymetric data over the Complex, means that best-fit profiles for the Great Meteor Seamount are not expected to produce simultaneously good fits for the Cruiser Complex. The horizontal scale bar, centred under the Great Meteor Seamount, represents a distance of 100 km and the vertical scale bar, centred around the best-fit profile, represents a topography of 2000 m.

elling over the Great Meteor Seamount. Bathymetric contour plots of the area show the seamount to possess a dimensionality of approximately 1:1, so from Fig. 1a, T_e^{true} can be read off as being approximately 12–17 km. This range compares with the published values from Watts et al. [35] of 18.5 km (or 21 km for the Young's modulus value given in Table 1) and from Verhoef [36] of approximately 20 km. Differences in these values were most likely caused by these authors setting $\rho_{\text{infill}} = \rho_{\text{load}}$ in their 2-D gravity modelling. Indeed, for higher ρ_{infill} values (e.g., 2700 kgm^{-3}), although the southern flank is accentuated, the T_e^{true} value obtained from the dimensionality plot would be ~ 19 km, very similar to these previously published results.

A 1-D method of recovering topography from the geoid can thus be used to provide useful estimates of elastic thickness values under seamounts. The use of the Great Meteor Seamount as a test case also serves to highlight the two main causes of differences between observed and recovered topographic profiles that may be experienced in modelling, that of poor bathymetric data coverage leading to artefacts in the gridded bathymetry, and of different elastic thickness values affecting different parts of each profile.

7. South central Pacific results

Although satellite ground tracks pass close to many of the south Pacific seamounts, the overall lack of surface ship bathymetric measurements excluded a number of these; seamounts such as Mururoa atoll and Mangaia Island were rejected on these grounds. Applying the three selection criteria, that of suitable surface ship bathymetric data, suitable satellite ground track coverage and known load and plate ages, to all the possible seamounts in the area reduced the overall number of seamounts acceptable for this study to ten and these are shown on the location map (Fig. 5). A total of 20 satellite altimetry profiles were analysed to obtain estimates of the along-track recovered elastic thickness values, T_e^{true} beneath these topographic loads and the quality of fit between the recovered and observed topographic profiles ranged from good to poor.

The loads fell into four groups (Fig. 5): (1) Society Islands—Tahiti, Huahine, Maupiti, Ra-

iatea-Tahaa; (2) Cook Islands—Aitutaki, Rarotonga; (3) Gambier Islands—Pitcairn, Gambier; and (4) Austral Islands—Maria, Macdonald. No other islands in the Austral chain satisfied all three selection criteria. Of these groups, the Society Islands had the highest density of observed bathymetric data. The ranges of parameters that produced best-fitting profiles of recovered topography for these ten seamounts are given in Table 2; Fig. 6 displays typical best-fit profiles for four of these loads, one from each group: Raiatea-Tahaa in the Society Islands; Rarotonga in the Cook Islands; Pitcairn in the Gambier Islands; and Maria in the Austral Islands.

The dimensionality studies in Section 3 showed

that seamounts having low 1-D along-track recovered elastic thickness values will likewise have low true elastic thickness values. Table 2 shows that, apart from Tahiti, all of the 1-D along-track recovered elastic thickness values are low. In order to enable the results obtained in this paper to be compared directly to those previously published it is necessary to correct the values for the effects of dimensionality listed in Table 2 and for this we used the results from the dimensionality modelling summarized in Fig. 1. These corrected elastic thickness values given in Table 2 are plotted in Fig. 7. We emphasize that the dimensionality corrections are not ideal since real seamounts do not possess perfect gaussian geometry and

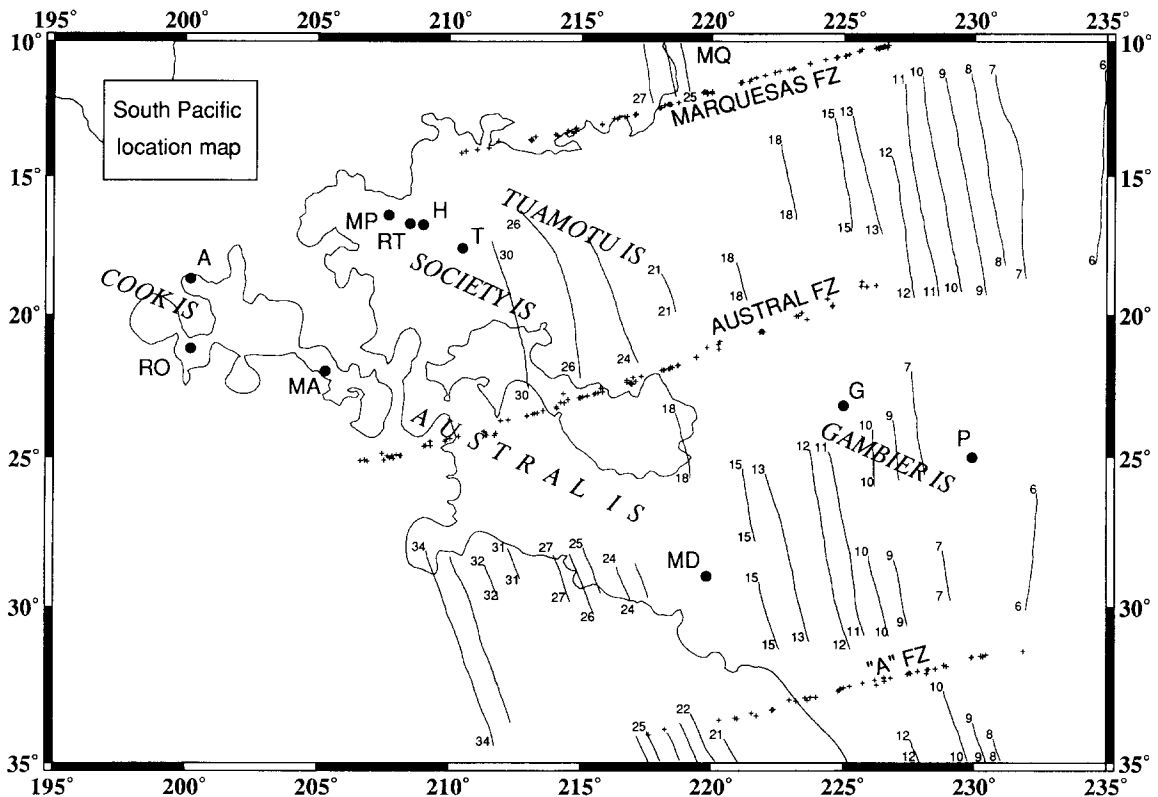


Fig. 5. Location map showing the positions (●) of the ten seamounts used in this study. The seamounts are labelled as follows: *SOCIETY IS*: T = Tahiti; H = Huahine; RT = Raiatea-Tahaa; MP = Maupiti. *COOK IS*: A = Aitutaki; RO = Rarotonga. *GAMBIER IS*: P = Pitcairn; G = Gambier. *AUSTRAL IS*: MA = Maria; MD = Macdonald. The Marquesas Islands lie to the north of the Marquesas fracture zone just off the top of the map at 220° longitude and are indicated by the letters MQ. Short solid lines trending almost N-S are the magnetic anomaly isochrons from Cande et al. [43] and small crosses give the location of major fracture zone picks (labelled) taken from Goodwillie and Parsons [44]. To indicate the extent of the regional depth anomaly, termed the South Pacific Superswell by McNutt and Fischer [6], the 4500 m bathymetric contour is also shown (small outcrops of this contour were removed from the plot to avoid cluttering). This bathymetric contour clearly extends far to the west whereas in "normal" oceanic basins it would be expected to follow the trend of the isochrons [45].

since the amplitudes and water depths of each seamount studied differ slightly from the model values. Figure 7a shows the results previously obtained by Calmant [2] in which low elastic thickness values were found to be associated with the seamounts of this region and Fig. 7b shows that low elastic thickness values for a number of these seamounts are confirmed by the results presented in this present study.

A striking feature of Fig. 7b is the clustering of data points having corrected elastic thickness values much lower than expected. Huahine, Maupiti, Raiatea-Tahaa, Maria, Pitcairn and Macdonald seamounts clearly display elastic thicknesses below their expected values. Four of these seamounts were studied by Calmant [2] and after re-calculating his thicknesses with a Young's modulus of 70 GPa (Fig. 7a), the values compare as follows: Maupiti, this study 4–7 km (Calmant, 16 ± 1 km); Maria, 4–7 km (12 ± 0.5 km); Pitcairn

< 4 km (≤ 5 km); Macdonald < 4 km (≤ 5 km). Comparison of the absolute values in these two studies must be done with caution since the corrections applied to our initial results were for theoretical models, most important is that both sets of these values are anomalously low. Previous studies have suggested that the most likely cause of these low elastic thickness values can be explained in terms of either lithospheric reheating which, in effect, resets the age of the lithospheric plate at the time of loading [37] or in terms of a thinner (75 km) lithospheric plate [5,6]. Though, as pointed out by Smith et al. [38], elastic thickness estimates alone are not able to distinguish between these two suggestions, with the additional information provided by depth anomalies and subsidence histories also being required.

The along-track elastic thicknesses of 10–14 km for the island of Aitutaki and 5–12 km for

TABLE 2

Ranges of the best-fit parameters for topographic recovery

load name	load age(Ma)	plate age(Ma)	dimension	half-width(km)	profile #	position	ρ_{infill} (kgm^{-3})	T_e^{rec} (km)	T_e^{true} (km)	T_e (km)	quality of fit
Tahiti	0.8 ¹	70 ²	2:1	65	1	flank	2.4–2.5	20–22	22–25	26	good
Huahine	2.3 ¹	74 ³	1:1	35	5	flank	2.4–2.5	5–9	7–17	27	good
Raiatea	2.5–2.9 ^{1,3}	74.5 ²	1:1	60	1	flank	2.6–2.65	8–10	9–12	27	good
Maupiti	4.3 ¹	76.5 ²	1:1	35	3	flank	2.4–2.7	3–5	4–7	27	fair
Maria	15.4 ⁴	80 ²	1:1	25	1	flank	2.4–2.6	3–5	4–7	25	good
Aitutaki	7.0 ⁵	87 ²	1:1	35	1	flank	2.2–2.5	10–14	> 21	29	poor
Rarotonga	1.5 ⁵	87 ²	1:1	30	3	centre	2.4–2.5	5–12	> 8	29	fair
Pitcairn	0.7 ⁶	23 ²	1:1	25	2	centre	2.6–2.7	0–2	< 4	15	good
Gambier	5.9 ⁶	30.5 ⁷	2:1	35	1	flank	2.4–2.7	7–11	11–25	16	fair
Macdonald	0 ⁸	42 ⁷	1:1	20	2	centre	2.6	1–3	< 4	21	good

Elastic thickness values for the ten south central Pacific seamounts after correction for the effects of dimensionality. The approximate dimensionality was obtained from contour maps of the gridded bathymetry, and the approximate halfwidths were taken as the mean values of the along-track halfwidths measured off the observed bathymetric profiles. The profile position gives the average position of the altimetric profiles in relation to the centre of the seamount. The T_e^{rec} and ρ_{infill} columns give the best-fitting range of parameters used for the 1-D along-track fit and the T_e^{true} column gives the corrected elastic thickness values that were read off from the dimensionality graphs. The second to last column lists the theoretical elastic thickness value, T_e , for each seamount which was taken as the depth to the 450°C isotherm of the cooling plate model. Load age and plate age values are referenced by the superscripts as follows:

¹ [46].

² [2].

³ Interpolated from Calmant [2].

⁴ Age assuming an average rate of migration of volcanism of 10.7 cm/yr [46] over a distance of 1650 km.

⁵ [47].

⁶ [48].

⁷ Interpolation between magnetic isochrons [43] using the timescale of Berggren et al. [49].

⁸ [50].

Rarotonga fall on that part of the 1:1 dimensionality curves in Fig. 1b for which no constraint can be placed upon the upper bound of the corrected

elastic thickness value, and in these cases it is only possible to give *minimum* corrected elastic thickness values of 21 and 8 km, respectively. The

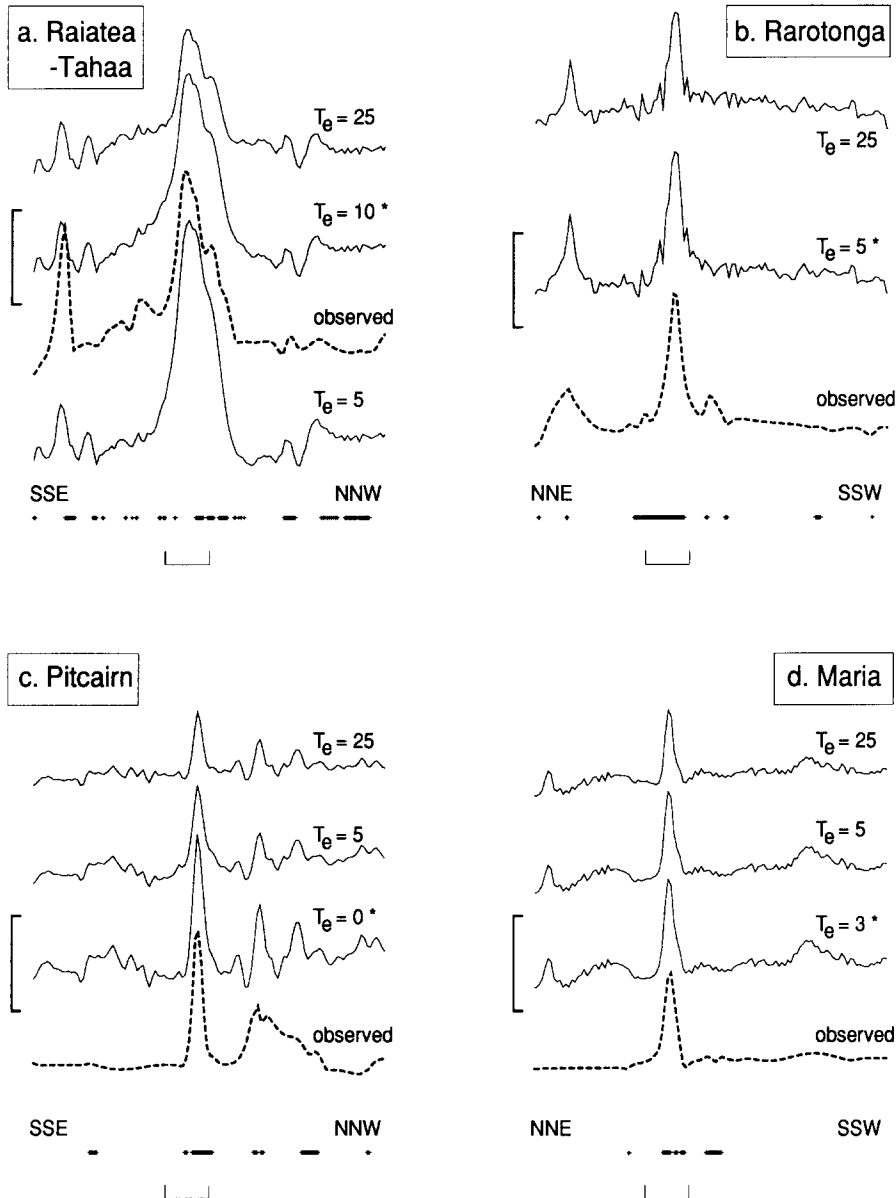


Fig. 6. Best-fit topographic profiles, indicated with an asterisk, recovered from the 1-D altimetric geoid height data for four named seamounts within the study area. In each plot the dashed profile shows the observed topography sampled along the same track line as the altimetry data and is plotted below the best-fit recovered topographic profile. The vertical scale bar, centred around the best-fit profile, represents a topography of 2000 m, and the horizontal scale bar, centred under the named seamount, represents a distance of 100 km. The remaining solid profiles show the recovered topography for elastic thicknesses of 25 and 5 km, typical of off-ridge and on-ridge volcanism respectively [23]. The density of the observed ship track bathymetric data lying within ± 7.5 km of the track line is plotted as crosses below the stack of topographic profiles. (a) Raiatea-Tahaa, ERS-1 track a008. (b) Rarotonga, ERS-1 track d258. (c) Pitcairn Island, Seasat track P0581. (d) Maria, Geosat track d243.

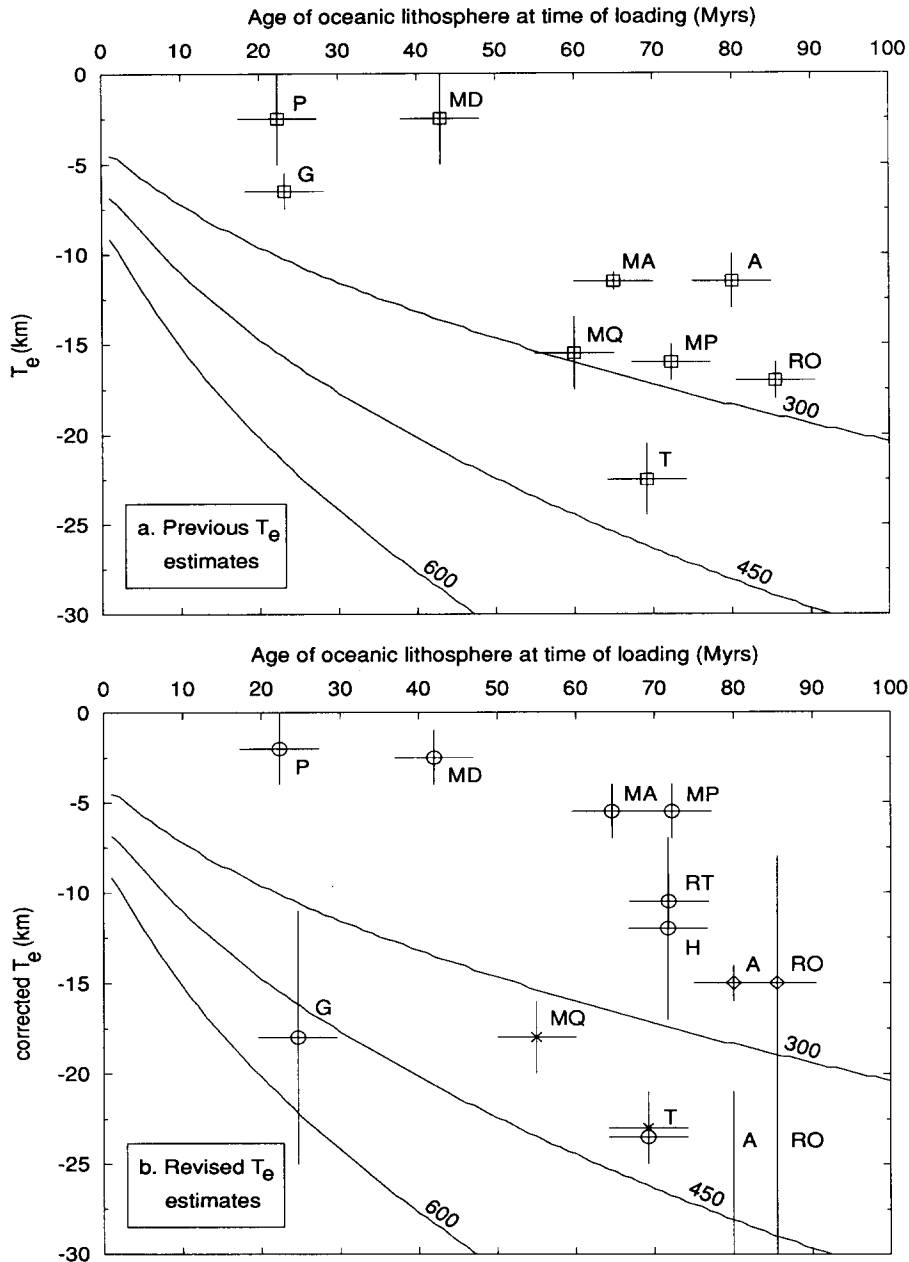


Fig. 7. Elastic thickness values for the south central Pacific seamounts mentioned in the text. Name labels are the same as in Fig. 5. Superimposed onto this plot are isotherms, labelled in °C, from the cooling plate model [45] in which the depth to the 450°C isotherm characteristically marks the base of the long-term elastic lithosphere [1]. (a) Previous estimates of elastic thickness values from Calmant [2] for the eight seamounts in the French Polynesia region common to both of our studies. Values have been re-calculated for a Young's modulus value of 70 GPa. Additionally, his determination for the Marquesas Islands (*MQ*) is also shown. (b) Revised elastic thickness values (○) using high-resolution altimetry for the ten seamounts used in this present study after correction for the effects of dimensionality. The two values for Aitutaki (*A*) and Rarotonga (*RO*) at approximately 85 My are interpreted as having minimum elastic thickness values of 21 and 8 km respectively. The values for these two seamounts obtained by McNutt and Menard [39] are shown (◇). Also plotted (×) are the elastic thickness results beneath the southeastern Society Islands (*T*) and the Marquesas Islands (*MQ*) from Filmer et al. [12].

results obtained by Calmant [2] for these two loads give elastic thicknesses in the range 10–13 and 16–18 km, respectively (Fig. 7a). McNutt and Menard [39] analysed uplift of surrounding atolls located on the flexural bulges and concluded that flexural rigidities for this area are in the range $1.7\text{--}2.5 \times 10^{22}$ Nm corresponding to an elastic thickness of 14–16 km for Aitutaki and Rarotonga (Fig. 7b).

Interestingly, Fig. 7b shows that, within the limitations of the correction process, some of the elastic thickness values are in fact normal. The corrected value for Tahiti (23.5 ± 1.5 km) is in close agreement to the expected value of 26 km and this compares well to previously published estimates of 24 km [40], 20 km [2] and 17 km [15], the latter low value being for load density between $2500\text{--}2700$ kgm⁻³. In addition, the most recent study of elastic thickness under the south-eastern Society Islands [12] shows that, for a load density of 2700 kgm⁻³, an elastic thickness estimate of approximately 23 km is most suitable (Fig. 7b). We consider this latter estimate to be the most accurate to date since Filmer et al. [12] used Sea Beam swath bathymetry to construct a new gridded bathymetry far superior in quality to the original SYNAPS data. From this surface they forward-modelled gravity anomalies and compared these anomalies with high-precision surface-ship gravity data collected along the same track lines as the Sea Beam bathymetry. Remodelling our data with a lower load density of 2700 kgm⁻³ would give a corrected elastic thickness in the range 25–28 km. Interestingly, Fig. 7b shows that for the Society Islands there is an almost linear decrease of elastic thickness value with distance from the hotspot under Mehetia which lies 150 km to the southeast of Tahiti.

The elastic thickness value for Gambier Island, previously found to be low by Calmant [2] (6.5 ± 1 km), is now interpreted to have a corrected value of 18 ± 7 km which is also in close agreement to the expected value of 16 km. Further, we speculate that previously low estimates for two other islands, 17 ± 1 and 14–16 km for Rarotonga, and 11.5 ± 1.5 and 14–16 km for Aitutaki [2,39] may now also plot nearer the 450°C isotherm with the values obtained in the present study, but the unconstrained nature of these results makes it difficult to infer further information.

8. Discussion

Previous work on elastic thickness values beneath seamounts in the south central Pacific, for instance by Calmant [2], indicated that almost all of the seamounts in this area are characterised by anomalously low values (Fig. 7a) and, combined with the well-documented depth anomaly [6], low sea floor subsidence rate [7] and lower than expected surface-wave velocities [5,9], these indicated a regional scale thermal anomaly beneath the south central Pacific Ocean. Smith et al. [38] have argued that the thermal anomaly is long-lived, giving rise to depth anomalies associated with Cretaceous-aged seamounts in the western Pacific.

Whilst a number of seamounts yield anomalously low elastic thickness values, the results presented in this paper show that Tahiti, Gambier, and perhaps Rarotonga and Aitutaki appear more normal. Another elastic thickness value originally taken as being low, that of 15.5 ± 2 km for the Marquesas Islands [2], has also recently been shown to be associated with an elastic thickness value closer to its expected value [12]. With the exception of the Marquesas Islands, these seamounts are located on a regional topographic swell termed the South Pacific Superswell by McNutt and Fischer [6]. Figure 5 shows that these islands are distributed throughout the superswell area and this suggests that for the remaining anomalous seamounts, lithospheric weakening and reheating is limited in its spatial extent. Stein and Abbott [4] compiled heat flow data covering much of the Pacific and reported that reheating of the upper lithosphere on a regional scale is not a feature of the superswell region. In order to account for the low elastic thickness values in this area, they suggested that one possible explanation could be due to local reheating occurring beneath the seamounts. Further, Fleitout and Moriceau [41] proposed numerous closely-spaced, thin rising plumes beneath the east-central Pacific to account for short-wavelength geoid anomalies in this area.

The possibility of local-scale variability is further supported by the results of geochemical analysis of rocks from islands in this region. Palacz and Saunders [11] presented combined Pb–Sr–Nd isotope and trace element data for eight islands

in the Cook–Austral–Samoa chain. They found that the islands of Rarotonga, Aitutaki and Atiu display characteristics of the Dupal component [42], having high isotope ratios for $^{87}\text{Sr}/^{86}\text{Sr}$, $^{207}\text{Pb}/^{206}\text{Pb}$, $^{208}\text{Pb}/^{206}\text{Pb}$, low ratios for $^{143}\text{Nd}/^{144}\text{Nd}$ and enrichment of Th relative to Ta. However, these authors found the adjacent island of Mangaia to be characterised by a distinctly different geochemical signature, termed the Mangaian component, with low $^{87}\text{Sr}/^{86}\text{Sr}$, high radiogenic Pb, and low trace element abundances but with high U. Hart [42] points to other such localised variations reported within the Azores and for the Koolau series in the Hawaiian chain. Smith et al. [38] showed that two of the Magellan seamounts in the western Pacific that display the Dupal and Mangaian geochemical components are found to backtrack to the present-day locations of the Rarotonga and Rurutu hotspots which are similarly characterised by these same geochemical components [11]. Dating the seamounts as Early Cretaceous led Smith et al. [38] to conclude that the mantle isotope source rocks must have existed in close geographical association for at least 100 Ma. Geochemical results therefore corroborate the idea of seamount individuality and, as yet, it remains unclear how these localised geochemical anomalies, together with the variability in the elastic thickness estimates, are related to the regional anomalies of the superswell region.

9. Conclusions

High-resolution, along-track altimetry data were combined with newly-gridded bathymetric data to study flexure of the lithosphere beneath ten seamounts in the south central Pacific Ocean. Six of the seamounts studied yielded lower than expected estimates of elastic thickness values whilst Tahiti and Gambier Island, and possibly also Aitutaki and Rarotonga, were best described using elastic thickness values that are in relatively good agreement with those expected. The apparent lack of any pattern in the geographical distribution of these two groups of seamounts, coupled with the results from previously published geochemical and heat flow data suggest that variations beneath seamounts in the south central Pacific Ocean occur on a localised scale and that there is no simple relationship between these

variations and the regional geophysical anomalies of the superswell region.

References

- 1 A.B. Watts, An analysis of isostasy in the world's oceans: 1. Hawaiian–Emperor seamount chain, *J. Geophys. Res.* 83, 5989–6004, 1978.
- 2 S. Calmant, The elastic thickness of the lithosphere in the Pacific Ocean, *Earth Planet. Sci. Lett.* 85, 277–288, 1987.
- 3 S. Calmant and A. Cazenave, The effective elastic lithosphere under the Cook–Austral and Society Islands, *Earth Planet. Sci. Lett.* 77, 187–202, 1986.
- 4 C.A. Stein and D.H. Abbott, Heat flow constraints on the south Pacific superswell, *J. Geophys. Res.* 96, 16,083–16,099, 1991.
- 5 M. McNutt and A.V. Judge, The superswell and mantle dynamics beneath the south Pacific, *Science* 248, 969–975, 1990.
- 6 M. McNutt and K.M. Fischer, The south Pacific superswell, in: *Seamounts, Islands, and Atolls*, B.H. Keating, P. Fryer, R. Batiza and G.W. Boechler, eds., *Am. Geophys. Union Geophys. Monogr.* 43, 25–34, 1987.
- 7 J.R. Cochran, Variations in subsidence rates along intermediate and fast spreading mid ocean ridges, *Geophys. J.R. Astron. Soc.* 87, 421–454, 1986.
- 8 W.F. Haxby and J.K. Weissel, Evidence for small-scale mantle convection from Seasat altimeter data, *Eos Trans. Am. Geophys. Union* 64, 838, 1983.
- 9 C.E. Nishimura and D.W. Forsyth, Anomalous Love-wave phase velocities in the Pacific: sequential pure path and spherical harmonic inversion, *Geophys. J.R. Astron. Soc.* 81, 389–407, 1985.
- 10 B. Dupre and C.J. Allegre, Pb–Sr isotope variation in Indian Ocean basalts and mixing phenomena, *Nature* 303, 142–146, 1983.
- 11 Z.A. Palacz and A.D. Saunders, Coupled trace element and isotope enrichment in the Cook–Austral–Samoa islands, southwest Pacific, *Earth Planet. Sci. Lett.* 79, 270–280, 1986.
- 12 P.E. Filmer, M.K. McNutt and C.J. Wolfe, Elastic thickness of the lithosphere in the Marquesas and Society Islands, in press.
- 13 W.H.F. Smith and P. Wessel, Gridding with continuous curvature splines in tension, *Geophysics* 55, 293–305, 1990.
- 14 A.B. Watts, On geoid heights derived from Geos 3 altimeter data along the Hawaiian–Emperor seamount chain, *J. Geophys. Res.* 84, 3817–3826, 1979.
- 15 K. Lambeck, Flexure of the ocean lithosphere from island uplift, bathymetry and geoid height observations: the Society Islands, *Geophys. J.R. Astron. Soc.* 67, 91–114, 1981.
- 16 W.J. Groeger, An experimental computer algorithm for seamount model parameter estimation based on Seasat-A satellite radar altimetry, *Techn. Rep.* 81-200, 50 pp., Naval Surface Weapons Center, Dahlgren, VA, 1981.
- 17 T.H. Dixon and M.E. Parke, Bathymetric estimates in the southern oceans from Seasat altimetry, *Nature* 304, 406–411, 1983.
- 18 T.H. Dixon, M. Naraghi, M.K. McNutt and S.M. Smith,

- Bathymetric prediction from Seasat altimeter data, *J. Geophys. Res.* 88, 1563–15711, 1983.
- 19 A.R. Lazarewicz and D.C. Schwank, Detection of uncharted seamounts using satellite altimetry, *Geophys. Res. Lett.* 9, 385–388, 1982.
 - 20 K. Lambeck and R. Coleman, A search for seamounts in the southern Cook and Austral region, *Geophys. Res. Lett.* 9, 389–392, 1982.
 - 21 A.B. Watts, J.R. Cochran, P. Patriat and M. Doucoure, A bathymetry and altimetry profile across the Southwest Indian Ridge crest at 31 S latitude, *Earth Planet. Sci. Lett.* 9, 129–139, 1985.
 - 22 S. Calmant, Inverse modelling of seamount topography using altimetric data and shipborn bathymetric and gravimetric data, *Eos Trans. Am. Geophys. Union* 73, 133, 1992.
 - 23 A.B. Watts and N.M. Ribe, On geoid heights and flexure of the lithosphere at seamounts, *J. Geophys. Res.* 89, 11,152–11,170, 1984.
 - 24 D. McKenzie, A. Watts, B. Parsons and M. Rofosse, Planform of mantle convection beneath the Pacific Ocean, *Nature* 288, 442–446, 1980.
 - 25 B. Parsons and S. Daly, The relationship between surface topography, gravity anomalies, and temperature structure of convection, *J. Geophys. Res.* 88, 1129–1144, 1983.
 - 26 A.B. Watts and S.F. Daly, Long wavelength gravity and topography anomalies, *Annu. Rev. Earth Planet. Sci.* 9, 415–448, 1981.
 - 27 M.E. Chapman, Techniques for interpretation of geoid anomalies, *J. Geophys. Res.* 84, 3793–3801, 1979.
 - 28 A.B. Watts, J.K. Weissel, R.A. Duncan and R.L. Larson, Origin of the Louisville Ridge and its relationship to the Eltanin Fracture Zone System, *J. Geophys. Res.* 93, 3051–3077, 1988.
 - 29 R.E. Cheney, B.C. Douglas, R.W. Agreen, L. Miller, D.L. Porter and N. Doyle, eds., *Geosat altimeter geophysical data record user handbook*. NOAA Techn. Mem. NOS NGS-46, Nat. Oceanogr. Atmos. Adm., US Dep. Commerce, Rockville, MD, 1987.
 - 30 B.D. Tapley and G.H. Born and M.E. Parke, The Seasat altimeter data and its accuracy assessment, *J. Geophys. Res.* 87, 3179–3188, 1982.
 - 31 P. Vass and M. Handoll, *UK ERS-1 Reference Manual*, Earth Observation Sciences, DC-MA-EOS-ED-0001, 1, Branksome Chambers, Fleet, 1991.
 - 32 J.G. Marsh, F.J. Lerch, B.H. Putney, D.C. Christodoulidis, D.E. Smith, T.L. Felsentreger, B.V. Sanchez, S.M. Klosko, E.C. Pavlis, T.V. Martin, J.W. Robbins, R.G. Williamson, O.L. Colombo, D.D. Rowlands, W.F. Eddy, N.L. Chandler, K.E. Rachlin, G.B. Patel, S. Bhati and D.S. Chinn, A new gravitational model for the earth from satellite tracking data: GEM-T1, *J. Geophys. Res.* 93, 6169–6215, 1988.
 - 33 R.D. Hyndman, N.I. Christensen and M.J. Drury, Velocities, densities, electrical resistivities, porosities, and thermal conductivities of core samples from boreholes in the islands of Bermuda and the Azores, in: *Deep Drilling Results in the Atlantic Ocean: Ocean Crust*, M. Talwani, C.G. Harrison and D.E. Hayes, eds., *Am. Geophys. Union M. Ewing Ser.* 2, 94–112, 1979.
 - 34 A.B. Watts and U.S. Ten Brink, Crustal structure, flexure, and subsidence history of the Hawaiian Islands, *J. Geophys. Res.* 94, 10,473–10,500, 1989.
 - 35 A.B. Watts, J.R. Cochran and G. Selzer, Gravity anomalies and flexure of the lithosphere: a three-dimensional study of the Great Meteor Seamount, northeast Atlantic, *J. Geophys. Res.* 80, 1391–1398, 1975.
 - 36 J. Verhoeve, A geophysical study of the Atlantis–Meteor seamount complex, *Geol. Ultraiectica* 38, 1984.
 - 37 M. McNutt, Lithospheric flexure and thermal anomalies, *J. Geophys. Res.* 89, 11,180–11,194, 1984.
 - 38 W.H.F. Smith, H. Staudigel, A.B. Watts and M.S. Pringle, The Magellan seamounts: early Cretaceous record of the south Pacific isotopic and thermal anomaly, *J. Geophys. Res.* 94, 10,501–10,523, 1989.
 - 39 M. McNutt and H.W. Menard, lithospheric flexure and uplifted atolls, *J. Geophys. Res.* 83, 1206–1212, 1978.
 - 40 A. Cazenave and B. Lago and K. Dominh and K. Lambeck, On the response of the ocean lithosphere to seamount loads from Geos 3 satellite radar altimeter observations, *Geophys. J.R. Astron. Soc.* 63, 233–252, 1980.
 - 41 L. Fleitout and C. Moriceau, Short wavelength geoid, bathymetry and the convective pattern beneath the Pacific Ocean, *Geophys. J. Int.* 110, 6–28, 1992.
 - 42 S.R. Hart, A large-scale isotope anomaly in the Southern Hemisphere mantle, *Nature* 309, 753–757, 1984.
 - 43 S.C. Cande, J. LaBreque, R.L. Larson, W.C. Pitman III, X. Golovchenko and W.F. Haxby, Magnetic lineations of the world's ocean basins (map with text), *Am. Assoc. Pet. Geol.*, Tulsa, OK, 1989.
 - 44 A.M. Goodwillie and B. Parsons, Placing bounds on lithospheric deformation in the central Pacific Ocean, *Earth Planet. Sci. Lett.* 111, 123–139, 1992.
 - 45 B. Parsons and J.G. Sclater, An analysis of the variation of ocean floor bathymetry and heat flow with age, *J. Geophys. Res.* 82, 803–827, 1977.
 - 46 R.A. Duncan and I. McDougall, Linear volcanism in French polynesia, *J. Volcanol. Geotherm. Res.* 1, 197–227, 1976.
 - 47 G.B. Dalrymple, R.D. Jarrard and D.A. Clague, Potassium–argon ages of some volcanic rocks from the Cook and Austral Islands, *Geol. Soc. Am. Bull.* 86, 1463–1467, 1975.
 - 48 R.D. Jarrard and D.A. Clague, Implications of Pacific island and seamount ages for the origin of volcanic chains, *Rev. Geophys. Space Phys.* 15, 57–76, 1977.
 - 49 W.A. Berggren, D.V. Kent, J.J. Flynn and J.A. Van Couvering, Cenozoic Geochronology, *Geol. Soc. Am. Bull.* 96, 1407–1418, 1985.